Journal of the Brazilian Society of Mechanical Sciences and Engineering (2018) 40:272
https://doi.org/10.1007/s40430-018-1176-7

REVIEW

Numerical investigation of the minimum fluidization velocity in a gas–solid fluidized bed using discrete phase model

M. Mehdizad[1] · R. Kouhikamali[1]

Received: 8 October 2017 / Accepted: 10 April 2018 / Published online: 2 May 2018

Abstract

The main purpose of this work is to find a new numerical model that is capable of investigating the minimum fluidization velocity in a gas–solid bed over a broad range of particle diameters and particle densities. In the present work, CFD simulation of a cylindrical gas–solid fluidized bed has been carried out using discrete phase model. Different drag correlations were examined to simulate the momentum between phases. Comparing the numerical values with the experimental values of the minimum fluidization velocity indicates that the drag models of Cheremisinoff and Gupta and Holzer and Sommerfeld have the least deviation, so they are suitable for modeling the drag forces of spherical and non-spherical particles, respectively. Experimental studies were carried out using a 10.5 cm cylindrical bed. The ranges of particles diameter and density vary from 10 μm to 10 mm and 6–6500 kg/m^3, respectively. Results showed that by 25% enhancement in diameter, density, crosswise sphericity coefficient, and sphericity of particles, the minimum fluidization velocity increases 94, 27, 12.5, and 3.5%, respectively. The numerical results of both spherical and non-spherical particles are in a very good agreement with experimental data within an average error of 6 and 9%, respectively.

Keywords Numerical simulation · Discrete phase model · Minimum fluidization velocity · Drag model · Gas holdup

List of symbols

a_1, a_2, a_3	Constant experimental coefficients
C_D	Drag coefficient
c_p	Specific heat coefficient (J/kg K)
D	Bed diameter (mm)
d_p	Particle diameter (μm)
d_v	Equivalent diameter of non-spherical particle (mm)
F_D	Drag force (N/kg)
F_x	Additional acceleration force (N/kg)
g	Gravitational acceleration (m/s^2)
g_x	Gravitational acceleration for the x direction (m/s^2)
h	Convective heat transfer coefficient (W/m^2 K)
h_{fg}	Latent heat coefficient (J/kg)
K	Thermal conductivity (W/m K)
m_p	Particle mass (kg)
$\dot{m}$	Mass flow rate (kg/s)
N_f	Archimedes number
P	Pressure (atm)
Re_s	Relative Reynolds number
T	Temperature (K)
u	Gas velocity (m/s)
u_{mf}	Minimum fluidization velocity (m/s)
u_p	Particle velocity (m/s)

Greek letters

ε	Gas holdup
φ	Sphericity
$\varphi_\perp$	Crosswise sphericity
μ	Dynamic viscosity (kg/m s)
ρ	Density (kg/m^3)
ψ	Drag coefficient ratio

Subscripts

f	Fluid
mf	Minimum fluidization
p	Particle
s	Single particle
z	Collections of particles

Technical Editor: Jader Barbosa Jr.

✉ R. Kouhikamali
kouhikamali@guilan.ac.ir

[1] Department of Mechanical Engineering, University of Guilan, Rasht 4193754741, Iran

1 Introduction

Gas–solid fluidized beds have some distinct properties that are imperative in today's industrial world especially in chemical engineering. Thorough mixing and large area contact between the gas and solid particles (which enables excellent heat and mass transfer between the bed and its container), uniform temperature gradients and frequent particle–particle and particle–wall collisions are some of these distinct properties. Hence, the gas–solid fluidized bed reactors have so many industrial applications such as catalytic cracking, metallurgy, gasification, uranium reduction, combustion, incinerator, drying, coating, etc.

Determining parameters that affect the minimum fluidization velocity (u_{mf}) requires performing specific experiments. Experiments carried out on cylindrical and 3D beds have shown that u_{mf} depends on bed and particle diameter and it is independent of bed height [1, 2], and experiments performed on 2D beds have indicated that u_{mf} is a function of the bed height, the particle diameter, and the column width [3]. Empirical correlations were suggested to determine the maximum pressure drop and the minimum fluidization velocity for gas–solid tapered fluidized beds were highly dependent on gas holdup and tapered angle [4]. Investigating the accuracy of these empirical correlations for predicting minimum fluidization velocity showed that most of these correlations depend on the bed characteristics and particle properties, but the effects of inter-particle forces were disregarded [5]. Correlations proposed for predicting the minimum fluidization velocity in 2D fluidized beds are usually dependent on the bed thickness and the particle diameter, ignoring the effect of inter-particle forces [6]. Correlations with the lowest deviation have been achieved by considering the influence of all effective factors include particle density, size, sphericity, bed geometry, static bed height, and inter-particle forces on hydrodynamic behavior of tapered fluidized bed [7]. Even though the effect of particle collisions has not been considered in most of these empirical correlations, they have shown desirable results. Since the aim of these works is only to investigate the minimum fluidization velocity and not to study the hydrodynamic behavior of fluidized beds comprehensively, the inter-particle forces do not have much significance at this level. Therefore, disregarding particle collisions would not affect the results. Investigating the effect of particle diameter, density, and sphericity on the minimum pick up velocity of binary mixtures in gas–solid pneumatic conveying showed that the impact of particle diameter on minimum pick up velocity is more dominant than particle density and the effect of particle sphericity was considerable [8]. Porosity is another essential factor in addition to the factors mentioned above, which has a significant impact on minimum fluidization velocities in both segregated and mixed beds. Mixed beds have a higher u_{mf} in comparison with segregated beds, since the lower porosity causes a higher pressure drop in mixed beds, which results in lower values of u_{mf} [9]. Kruggel-Emden and Vollmari [10] experimentally examined the bed height and pressure drop of Geldart group D non-spherical particles. Simulations of non-spherical particles in this work are validated by their experimental results.

To obtain better efficiency and have an accurate design with lower cost, the minimum fluidization velocity can be predicted using CFD modeling. Two different methods have been mainly used to apply CFD modeling to gas–solid fluidized beds: Eulerian–Lagrangian approach based on particle dynamics; and Eulerian–Eulerian approach based on continuum mechanics.

In Eulerian–Eulerian approach, both phases are treated as fully interpenetrating continuum. Modeling the transport coefficients of the particle–particle collisions and gas–particle interactions is the major problem, while the particulate phase is represented as a continuum. Obtaining a momentum balance for the dispersed phase necessitates so many assumptions, because the resultant continuum approximation has an uncertain determination of variables such as viscosity and normal stress for the solid phase [11]. Investigations of the hydrodynamics of 2D gas–solid fluidized beds using Eulerian–Eulerian approach have shown that Syamlal-O'Brien drag model is the most appropriate model for simulating these types of beds [12], and as the mass fraction increases, the bed height increases, but the average diameter of the mixture of particles decreases [13]. The same study was carried out on a gas–solid tapered fluidized bed and a circulating fluidized bed by applying the kinetic theory of granular flow, and the Gidaspow drag model was chosen as a suitable model to calculate the momentum between phases [14, 15]. However, simulating the fluidization behavior of a gas–solid micro fluidized bed using Eulerian–Eulerian approach to predict minimum bubbling velocity and bed voidage indicated that the results of Gidaspow drag model were lower than experimental data and the modified Gibilaro drag model is suitable. Besides, the parametric studies represented that the boundary condition of the particle–wall interactions had a considerable effect on the predicted gas and solid flow behavior [16].

In Eulerian–Lagrangian approach, the gas phase is treated as a continuum and the particles are tracked through the calculated flow field by solving the Newtonian equations of motion for each individual particle. Therefore, this approach does not need additional equations for the solid phase. Two approaches are widely used in characterizing particle–particle collisions: the hard sphere [17] and the

soft sphere approach [18]. It has been indicated in many experimental sources that discrete phase model is a very powerful tool to provide detailed information of dominant flow in fluidized beds due to its ability in calculating collision forces [19]. To study the behavior of non-spherical particles in a gas–solid fluidized bed, DEM simulation of non-spherical particles is coupled with pressure gradient force. In this method, the drag correlation of Holzer and Sommerfeld [20] is coupled with Di Felice [21] approach to consider the influence of porosity [22]. Investigating the relationships between pressure drop and gas superficial velocity, and microscopic parameters such as coordination number, particle orientation and force structure using the CFD–DEM method to study the fluidization of ellipsoidal particles have shown that particle shape significantly affects bed permeability and the minimum fluidization velocity [23].

Gas–solid fluidized beds are used broadly in heat exchangers, combustions, and reactors. One of the distinct properties of fluidized beds is the frequent particle–particle and particle–wall collisions, which increases heat transfer. In a cylindrical bed (which only contains fluid), the heat transfer occurs through the boundary layer. On the other hand, in gas–solid flows, solid particles receive the heat from the wall and turn into heat sources themselves, and transfer the heat by colliding to each other. Therefore, the heat transfer would increase and the heat would diffuse uniformly through the cylinder. Some properties such as particle diameter or density have a great impact on increasing the heat transfer. It is important to know how much these effective parameters could be increased without affecting the fluidization. Therefore, it is necessary to find a new cost-effective model to investigate the minimum fluidization velocity in a broad range of particle diameter and particle density; otherwise, it needs so many expensive experimental works. Hence, in this work, CFD simulation of a gas–solid fluidized bed has been carried out and the effects of diameter, density, and sphericity of solid particles on the minimum fluidization velocity have been studied using discrete phase model. CDF simulations need experimental comparisons to validate the presented model. After validation, the offered numerical model can be employed to predict minimum fluidization velocity of thousands of cases including particles with different shapes, diameters, and densities, which are too expensive to experiment individually. Several drag correlations have been examined to choose an appropriate drag model for calculating the momentum exchange between phases. The minimum gas holdup needed for occurring incipient fluidization has been specified based on comparisons between the numerical results and the experimental data for both spherical and non-spherical particles.

2 Experimental setup

Figure 1 shows the fluidized bed unit H692 manufactured in P.A. HILTON LTD available in the laboratory of the University of Guilan. The panel of this unit is one piece G.R.P. molding on which all components are mounted. The bedchamber is a strong glass cylinder with the internal diameter of 105 and 220 mm long, closed at the lower end by an air distribution system and at the upper end by a filter assembly. The chamber assembly is suspended from a stainless steel bracket. The bracket carries a heating element, thermocouple and pressure probe, all of which can be moved vertically within the chamber. Air from the local compressed air supply is delivered through a filter/pressure regulator, an air flow meter adjusted with a control valve and an orifice plate (to measure higher flow rates), to the distribution chamber. High airflow rates through the bed may cause some of the bed material to be transferred into the filter. Most of this will be returned to the bed when the airflow is reduced and the return may be assisted by gently tapping the outside of the filter. Two liquid filled manometers are set. One indicates the pressure of the air at any level in the bedchamber, and the other indicates the orifice differential pressure, which determines the higher airflow rates. The function of the air pressure regulator is to provide the bed with clean moisture free air and to provide a stable air pressure so that the variations in the local supply pressure do not affect the airflow rate through the bed.

The air flow meter has been calibrated for air at 101.3 kN/m^2 and 20 °C ($\rho = 1.205\text{kg m}^{-2}$, $\vartheta = 1.823 \times 10^{-5}$).

Provided changes of viscosity are small (say between 15 and 30 °C) the flow rate at other conditions can be calculated from

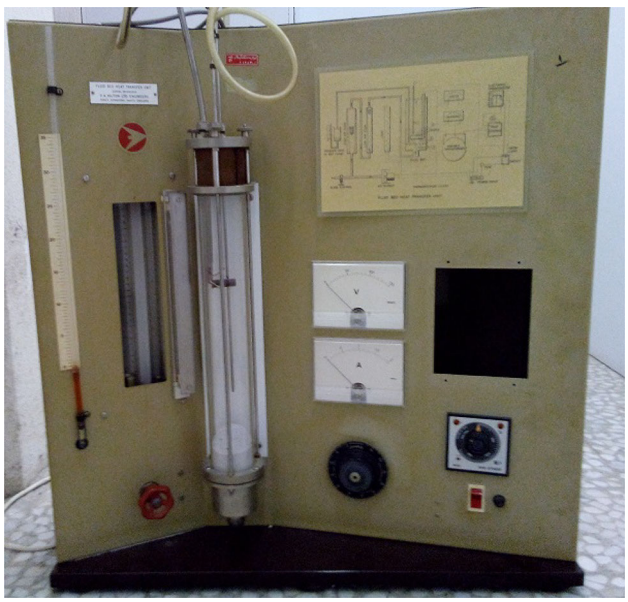

Fig. 1 Fluidized bed unit H692

$$\text{Actual flow rate} = \text{Indicated flow rate} \times \sqrt{\frac{1.205}{\rho_m}}, \quad (1)$$

where ρ_m is the density of the air in the meter in kg/m^2.

The pressure of the air in the meter is atmospheric pressure plus the resistances of the bed, distributer, pipe work, and orifice. Typically, this resistance is about 2.5 kN/m^2, but will vary with the flow rate. However, the effect of changes of pressure and temperature on the flow meter reading correction ($\sqrt{\frac{1.205}{\rho_m}}$) is insignificant at normal atmospheric pressure.

The distribution chamber is at the lower end of the cylinder, which is designed to support the bed when it is defluidized. This distributor has been set to ensure uniform gas flow through the bed without producing excessive pressure drop and is appropriate for the granular material supplied. The distributor consists of six discs of filter paper sandwiched between two stainless steel gauze discs; all being closed by a U-shaped rubber ring seal. The distribution (installed at the bottom of the system) provides adequate backpressure to ensure uniform air velocity through the entire cross-sectional area of the bed.

We charged a sufficient mass of the selected granular material into the bedchamber and remounted all components. Then, we set the airflow to a high value and let the bed mix thoroughly for two or three minutes. We record the bed height and the pressure drop across the bed (i.e., the difference between pressures indicated with the probe at its highest and lowest positions) without changing the airflow. After that, we reduced the airflow rate in steps and repeated the observations at each setting. By drawing the height and Δp against flow rate graphs as the experiment proceeds, the magnitude of the decrements can be estimated.

We reduced the flow rate to zero, and then sharply tap the bedchamber with the knuckles until the bed reached a minimum height. We repeated all the observations as the airflow is increased in similar steps.

The uncertainties were estimated using the method suggested by Bell [24] and Moffat [25]. The measurement uncertainties of the particles and airflow rates were ± 4.0 and ± 1.9%, respectively. The schematic design of the experimental setup is shown in Fig. 2.

3 CFD modeling

The CFD simulation approach implemented in this work is based on discrete phase model. In this model, the Navier–Stokes equations are solved for the continuous phase, a large number of particles are tracking through the calculated flow field to solve the particulate phase, and drag forces have been well calculated by applying suitable drag

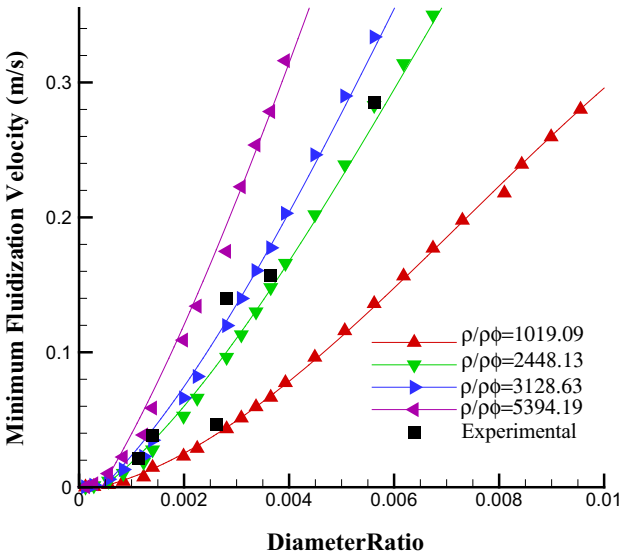

Fig. 2 Effect of diameter ratio on the minimum fluidization velocity under different density ratios

model. The particle–wall contact is realized by considering reflect boundary condition which allows particles get back to the flow after hitting the wall. The applied methodology is not a DEM but an approach similar to DEM neglecting particle–particle contact forces. DEM has longer runtime than DPM because of considering all contact forces. First, particles need to settle down row by row to make the bed, this step (modeling the bed) takes so much time itself, then fluid flow enters and makes every single particle fluidized. Fluidizing solid particles one by one and row by row and simulating all the contact forces between particles need so much time. At minimum fluidization velocity, fluid flow occupies the empty spaces between particles, and particles do not rest on each other anymore. However, they do not move at this velocity of the fluid. Since the purpose of this work is only to find the minimum fluidization velocity of particles in a fluidized bed, not to provide a detailed simulation of gas–solid flow in a fluidized bed, so the contact forces could be negligible at this stage of fluidization using a suitable modeling. In discrete particle method, the values of the diameter and density of solid particles and the total injected flow rate are defined. The number of particles would be calculated for each case, which can be different from case to case. Since the aim of this work is to study the effect of diameter and density of the particles (not their numbers), so the comparison of the numerical results with experimental values is based on the same diameters and densities. Simulations were performed on a desktop PC equipped four processors (Intel(R) Core(TM) i5-4200 CPU @ 1.6 GHz) and 8 GB of memory. The length of time required to compute the results for each simulation varied, but was typically between 3 and 4 h for the residuals of

continuity, x-velocity, and y-velocity to reach a reasonable amount and the transient solution to approach the steady-state solution asymptotically.

3.1 Computational geometry and boundary conditions

In this work, the discrete phase model was applied to simulate the cylindrical gas–solid fluidized bed with a vertical tube. Using DPM, a particulate phase can be simulated in a Lagrangian framework, in addition to solving transport equations for the gas phase. The discrete phase is composed of solid particles scattered in the continuous phase. DPM calculates the trajectories of these solid particles. The coupling between the particulate phase and the gas phase and its impact on the granular flow can be included. We used the following options of the discrete particle method:

- calculation of the particles trajectories using a Lagrangian frame, which covers the dispersed phase inertia, hydrodynamic drag, and the force of gravity;
- prediction of the effects of turbulence on the distribution of solid particles due to turbulent eddies present in the gas phase;
- two-way coupling of the gas phase prediction to the particulate phase calculations;
- consideration of particle/wall collisions and voidage of continuous phase.

In this simulation, it is assumed that particle injection occurs at inlet using surface type in the same direction as air moves (co-current flow). Reflect boundary condition of particle–wall collisions was chosen to return the particle back to the flow after the collision. The inlet boundary condition is the gas velocity and the outlet boundary condition is the constant pressure. The no slip boundary condition is considered at the wall. The numerical solution is based on the finite volume method. Equations of momentum and pressure were discretized using second-order upwind scheme and solved by the SIMPLE algorithm (pressure–velocity coupling). The unsteady particle tracking was performed using automated tracking scheme (high-order scheme: trapezoidal, and low order scheme: implicit) with the tolerance of 10^{-5}. There are two approaches for coupling the phases. One-way coupling in which fluid phase influences particulate phase via drag force and turbulence, but the dispersed phase has no influence on the gas phase. Two-way coupling that particulate phase also influences fluid phase via source terms of mass, momentum, and energy. The two-way coupling was applied in this work. Table 1 represents parameters and conditions of the CFD simulation.

Table 1 Simulation model parameters

Parameters	Value
Cylinder height (mm)	300,220
Cylinder diameter (mm)	89,105
Particle diameter range (μm)	10–1000
Particle density range (kg/m^3)	6–6500
Gas density (kg/m^3)	1.205
Gas viscosity (kg/ms)	1.823×10^{-5}
Ambient pressure (atm)	1
Grid spacing (mm)	0.2
Time step (s)	0.0001

3.2 Drag models

Minimum fluidization velocity is derived from equating the drag and pressure forces on the particle to their weight. Therefore, the drag force between particles and the gas phase has a dominant influence on the minimum fluidization velocity. Using the proper drag model is necessary to determine the drag force on the particle correctly. Therefore, many drag models have been introduced in articles for modeling the momentum between phases. In Tables 2 and 3, some of them that currently have been used as a successful model were collected.

These models are single particle models, which are not directly applicable for calculating momentum exchange between phases. Therefore, we assumed different possible values of the porosity based on experimental data, and we implemented the simulations several times for each material with different densities and diameters to determine the suitable primary value of porosity. Drag forces are dependent on drag coefficient of the group of particles, which is defined as a function of primary porosity $(\psi(\varepsilon))$ multiplied to single particle drag coefficient ($C_{\mathrm{D_s}}$, coefficients listed in Tables 2 and 3). Therefore, as it shown in Eq. (2), the drag coefficient of a mass of particles is defined as

$$C_{\mathrm{D_z}} = \psi(\varepsilon) \cdot C_{\mathrm{D_s}}, \quad \psi(\varepsilon) = \varepsilon^{-4.7}. \tag{2}$$

The sphericity (φ) represents the ratio between the surface area of the volume equivalent sphere and that of the considered particle. The crosswise sphericity ($\varphi_{\perp}$) is the ratio between the cross-sectional area of the volume equivalent sphere and the projected cross-sectional area of the considered particle. Re_{s} for non-spherical particles is defined as

$$Re_{\mathrm{s}} = \frac{\rho_{\mathrm{f}} \cdot u_{\mathrm{mf}} \cdot d_{\mathrm{v}}}{\mu}, \tag{3}$$

where d_{v} is the diameter of a sphere having the same volume as the particle. In Ganser correlation [24], k_1 and k_2 are functions of the sphericity, as they are shown in Eqs. (4) and (5):

Table 2 Different drag models for spherical particles

Model	Equation
Kelessidis [26]	$C_{D_s} = \frac{24}{Re_s} \quad Re_s < 1$
	$C_{D_s} = 18.5 Re_s^{-0.6} \quad 1 < Re_s < 500$
	$C_{D_s} = 0.44 \quad Re_s > 500$
Schiller and Naumann [27]	$C_{D_s} = \frac{24}{Re_s}\left(1 + 0.15 Re_s^{0.687}\right) \quad Re_s < 1000$
	$C_{D_s} = 0.44 \quad Re_s \geq 100$
Dallavalle [28]	$C_{D_s} = \left[0.63 + \frac{4.8}{\sqrt{Re_s}}\right]^2 \quad Re_s < 2 \times 10^5$
Morsi and Alexander [29]	$C_{D_s} = a_1 + \frac{a_2}{Re_s} + \frac{a_3}{Re_s^2}$
	$a_1, a_2, a_3 = \begin{cases} 0, 24, 0 & 0 < Re_s < 0.1 \\ 3.69, 22.73, 0.0903 & 0.1 < Re_s < 1 \\ 1.222, 29.1667, -3.8889 & 1 < Re_s < 10 \\ 0.6167, 46.5, -116.67 & 10 < Re_s < 100 \\ 0.3644, 98.33, -2778 & 100 < Re_s < 1000 \\ 0.357, 148.62, -47500 & 1000 < Re_s < 5000 \\ 0.46, -490.456, 578700 & 5000 < Re_s < 10,000 \\ 0.5191, -1662.5, 5416700 & 10,000 \geq Re_s \end{cases}$
Clift et al. [30]	$C_{D_s} = \frac{24}{Re_s} \quad Re_s < 0.01$
	$C_{D_s} = \frac{24}{18 Re_s}\left(18 + 2.367 Re_s^{0.82 - 0.05 \log Re_s}\right) \quad 0.01 < Re_s < 20.0$
	$C_{D_s} = \frac{24}{18 Re_s}\left(18 + 3.483 Re_s^{0.6305}\right) \quad 20 < Re_s < 260$
Ihme et al. [31]	$C_{D_s} = \frac{24}{Re_s} + 5.48 Re_s^{-0.573} + 0.36 \quad Re_s < 10^4$
Cheremisinoff and Gupta [32]	$C_{D_s} = \frac{24}{Re_s} \quad Re_s < 3$
	$C_{D_s} = \frac{24}{Re_s} + \frac{4}{Re_s^{1/3}} \quad 3 < Re_s < 500$
	$C_{D_s} = 0.44 \quad Re_s > 50$
Khan and Richardson [33]	$C_{D_s} = 2\left(\frac{1.84}{Re_s^{0.31}} + 0.293 Re_s^{0.06}\right)^{3.45} \quad 0.01 < Re_s < 3 \times 10^5$

Table 3 Different drag models for non-spherical particles

Equation	Model
Holzer and Sommerfeld [20]	$C_{D_s} = \frac{8}{Re_s}\frac{1}{\sqrt{\varphi_\perp}} + \frac{16}{Re_s}\frac{1}{\sqrt{\varphi}} + \frac{3}{\sqrt{Re_s}}\frac{1}{\varphi^{3/4}} + 0.42 \times 10^{0.4(-\log(\varphi))^2}\frac{1}{\varphi_\perp}$
Ganser [24]	$C_{D_s} = \frac{24}{Re_s k_1}\left\{1 + 0.1118(Re_s k_1 k_2)^{0.6567}\right\} + \frac{0.4305 k_2}{1 + \frac{3305}{Re_s k_1 k_2}}$
Swamee and Ojha [34]	$C_{D_s} = \left[\frac{48.5}{(1 + 4.5\beta^{0.35})^{0.8} Re_s^{0.64}} + \left\{\left(\frac{Re_s}{Re_s + 100 + 100\beta}\right)^{0.32}\frac{1}{\beta^{18} + 1.05\beta^{0.8}}\right\}\right]$
Chien [35]	$C_{D_s} = \left(\frac{30}{Re_s}\right) + 67.289\exp(-5.03\varphi)$
Haider and Levenspiel [36]	$C_{D_s} = \frac{24}{Re_s}\left(1 + A Re_s^B\right) + \frac{C}{1 + \frac{D}{Re_s}}$

$$k_1 = \left[\left(d_v/3d\right) + \left(\frac{2}{3}\right)\varphi^{-0.5}\right]^{-1}, \tag{4}$$

$$k_2 = 10^{1.8148(-\log\varphi)^{0.5743}}. \tag{5}$$

In Haider and Levenspiel [36] correlation, A, B, C, and D are given by

$$A = \exp(2.3288 - 6.4581\varphi + 2.4486\varphi^2), \tag{6}$$

$$B = 0.0964 + 0.5565\varphi, \tag{7}$$

$$C = \exp(4.905 - 13.8944\varphi + 18.42222\varphi^2 - 10.2599\varphi^3), \tag{8}$$

$$D = \exp(1.4681 + 12.2584\varphi - 20.7322\varphi^2 + 15.8855\varphi^3). \tag{9}$$

3.3 Model formulation

To model the fluidization phenomenon, at first, the initial position, velocity, density, and the diameter of individual particles are defined, and then, trajectories of the

particulate phase are calculated by the force balance on the particle and the local continuous phase conditions. The determination of the minimum fluidization velocity, formulations of the continuous phase, and the force balance on the particle are described below.

3.3.1 Continuous phase equations

Equations (10) and (11) represent transient transport equations for mass and momentum in the continuous phase, respectively [37]:

$$\frac{\partial \rho}{\partial t} + \frac{\partial}{\partial x_i}(\rho u_i) = M, \tag{10}$$

$$\frac{\partial}{\partial t}(\rho u_j) + \frac{\partial}{\partial x_i}(\rho u_i u_j) = \rho g_j - \frac{\partial P}{\partial x_j} + \frac{\partial}{\partial x_i}\left(\tau_{ij} - \rho\overline{u_i' u_j'}\right) + F. \tag{11}$$

Reynolds stresses were indicated by $\overline{\rho u_i' u_j'}$. τ_{ij} is symmetric stress tensor that can be calculated by [37]

$$\tau_{ij} = \mu\left(\frac{\partial u_j}{\partial x_i} + \frac{\partial u_i}{\partial x_j} - \frac{2}{3}\delta_{ij}\frac{\partial u_k}{\partial x_k}\right). \tag{12}$$

M and F are source/sink terms of mass and momentum that are exchanged between discrete and continuous phase. In fact, the impact of discrete phase on the continuous phase is considered in the equations of the continuous phase due to these terms. In this system, the mass source term is zero ($M = 0$) and the momentum source term is defined as follows [37]:

$$F = \sum\left(\frac{18\mu C_{\mathrm{D}} Re_{\mathrm{s}}}{\rho_{\mathrm{p}} d_{\mathrm{p}}^2 24}(u_{\mathrm{p}} - u) + F_{\mathrm{other}}\right)\dot{m}_{\mathrm{p}}\Delta t, \tag{13}$$

where $\dot{m}_{\mathrm{p}}$ are the change in the mass flow rate of the solid particles.

3.3.2 Discrete phase equations

Particle trajectory can be determined by integrating the force balance on the particle. Equation (14) represents this force balance in the Lagrangian form [37]:

$$\frac{\mathrm{d}u_{\mathrm{p}}}{\mathrm{d}t} = F_{\mathrm{D}}(u - u_{\mathrm{p}}) + \frac{g_x(\rho - \rho_{\mathrm{p}})}{\rho_{\mathrm{p}}} + F_x, \tag{14}$$

where $\frac{g_x(\rho_{\mathrm{p}} - \rho)}{\rho_{\mathrm{p}}}$ is the gravitational term and F_x expresses the additional forces that can be important under certain conditions such as virtual mass force, thermophoretic force, Brownian force, Saffman's lift force. These additional forces are disregarded in this study.

$F_{\mathrm{D}}(u - u_{\mathrm{p}})$ is the drag force per unit particle mass and F_{D} is defined as

$$F_{\mathrm{D}} = \frac{18\mu}{\rho_{\mathrm{p}} d_{\mathrm{p}}^2}\frac{C_{D_z} Re_{\mathrm{s}}}{24}, \tag{15}$$

where C_{D_z} is the drag coefficient for groups of particles and Re_{s} is the relative Reynolds number, which is specified as follows:

$$Re_{\mathrm{s}} = \frac{\rho d_{\mathrm{p}}|u_{\mathrm{p}} - u|}{\mu}. \tag{16}$$

3.3.3 Fluidization equations

Minimum fluidization velocity is the fluid volumetric flux at which the bed first becomes fluidized. At the minimum fluidization velocity, the drag and pressure forces on the particles equal their weight. Since the numerical values must be in the range of experimental values if the simulations are performed correctly, we inputted an initial value for the gas velocity, which was close to the experimentally calculated value ($0.75 \times$ experimentalvalue). This initial value could be any possible amount. We chose this value to speed up the process. At this value of gas velocity, particles remained motionless. By increasing the gas velocity gradually within an scale of 0.001 (since the highest precision of experimental data was 0.001, we took this scale to reduce the error as possible as we could), the velocity of the particles changed from zero to a very small amount (e.g., 0.00001) which proves that particles begin to move, but no considerable motion was captured in the particle trajectory. By applying additional enhancement on a scale of 0.001 to the gas velocity, the motion of particles could be seen in their trajectories. Since the minimum fluidization velocity is defined as the minimum gas velocity at which the bed first becomes fluidized, so the previous value of the gas velocity (the one in which particles begin to move, but no motion is captured in the particle trajectory) has been selected as the minimum fluidization velocity.

The equations mentioned in this section are used for calculating the minimum fluidization velocity [38]:

$$\left(C_{\mathrm{D}_z} \cdot Re_{\mathrm{s}}^2\right)_{\mathrm{mf}} = \frac{4}{3} \times N_{\mathrm{f}}^2, \tag{17}$$

where N_{f} is the Archimedes number which is represented as follows [38]:

$$N_{\mathrm{f}}^2 = \frac{\rho_{\mathrm{f}} \times d_{\mathrm{p}}^3 \times g \times (\rho_{\mathrm{s}} - \rho_{\mathrm{f}})}{\mu^2}, \tag{18}$$

where C_{D_z} is the drag coefficient for groups of particles that have accumulated on each other. The available drag coefficients are defined for a single particle. The ratio between the drag force for collections of particles and that of a single particle with the same volumetric flux is defined as [38]

$$\psi(\varepsilon) = \frac{C_{D_z}}{C_{D_s}}. \quad (19)$$

The approximate equivalent of this coefficient proposed by Wallis is $\varepsilon^{-4.7}$ (ε is the gas holdup) [38]. Therefore, Eq. (17) turns to

$$\left(C_{D_s} \cdot Re_s^2\right)_{mf} = \frac{4}{3} \times \varepsilon^{4.7} \times N_f^2. \quad (20)$$

3.4 Turbulence model

The flow regime can be laminar or turbulence based on the velocity of the continuous phase. In the case of having turbulence regime, choosing the proper turbulence model is one of the main factors that affect the accuracy of the numerical simulation. Different turbulence models including different $k-\varepsilon$ and $k-\omega$ models, Reynolds stress model, and scale adaptive simulation have been investigated, and ultimately, the most appropriate turbulence model was chosen due to comparisons between the numerical results and the experimental results of Gunn and Hilal [1]. However, the obtained deviations are very similar, but according to the importance of gas–particle interaction (drag forces) and particle–wall interaction in the present work, the final model should be able to properly model the both regions near the wall and away from the wall. By considering this fact and the runtime of each model, the shear stress transport $k-\omega$(SST) model was selected as a suitable model for turbulent flow modeling in this study. Table 4 represents the results of investigating different turbulence models for a sample case with the diameter of 175 μm and the density of 3770 kg/m^3.

3.5 Mesh independency

Five different grids listed in Table 5 were used for the Gunn and Hilal [1] and our cases to confirm that the prediction results are independent of the grid size. As shown in Table 5, the grid size of 0.2 mm and the grid size of 0.05 mm predicted similar minimum fluidization velocity for a sample case with 175 μm diameter and 3770 kg/m^3 density. Consequently, the grid size of 0.2 mm was used for the following calculations.

3.6 Model solution procedure

CFD simulations are carried out using the FLUENT software and the DPM model was included into this software is commercial. Under-relaxation factors were adjusted 0.3 for the equation of pressure and 0.7 for momentum, 0.8 for turbulence variables, and 0.5 for sources of mass and momentum. A time step of 0.0001 with 20 iterations per time step was chosen and the procedure continued until the steady state was obtained. We used standard initialization and we considered following initial conditions for time marching in our simulations: Gauge pressure: 0 (Pascal), axial velocity: equals to the inputted gas velocity value (m/s), radial velocity: 0 (m/s). Due to axisymmetric condition, half of the computational domain was discretized by 133,500 and 115,500 quadrilateral cells for the bed with the diameter of 105 and 89 mm, respectively.

Table 4 Comparisons of different turbulence models

Turbulence model	u_{mf} (m/s) (numerical)	u_{mf} (m/s) (experimental)	Errors (%)
Standard $k-\varepsilon$	0.069	0.0720	4.14
RNG $k-\varepsilon$	0.0676	0.0720	6.17
Realizable $k-\varepsilon$	0.0673	0.0720	6.53
Standard $k-\varepsilon$	0.0697	0.0720	3.25
SST $k-\varepsilon$	0.074	0.0720	2.78
Reynolds stress	0.068	0.0720	5.56
Scale adaptive simulation	0.0678	0.0720	5.77

Table 5 Grid independence study

Grid size (mm)	Number of cells	u_{mf} (m/s) (numerical)	u_{mf} (m/s) (experimental)	Errors (%)
1	26,700	0.07536	0.0720	4.67
0.5	53,400	0.07468	0.0720	3.72
0.25	106,800	0.07448	0.0720	3.45
0.2	133,500	0.07400	0.0720	2.78
0.05	534,000	0.07395	0.0720	2.71

4 Results and discussion

In this work, discrete phase model was applied to simulate a cylindrical gas–solid fluidized bed. The SST $k-\omega$(SST) model was selected as a turbulence model. Several drag models are examined to choose the most accurate model to obtain the best results for calculating the minimum fluidization velocity. The minimum gas holdup needed for occurring incipient fluidization for both spherical and non-spherical particles is determined based on comparisons with experimental data. The effects of particle sphericity, diameter, and density and the effect of the gas holdup on the minimum fluidization velocity were studied.

4.1 Validation of models

Numerical models developed in this work are validated by two experimental works: the experimental study that we performed using fluidized bed unit H692, and the experimental results of Gunn and Hilal [1].

Nine packs of different fused alumina (white aluminum oxide) loose granules are supplied. Properties of these packs are shown in Table 6.

To measure the minimum fluidization velocity, at first, a sufficient quantity of particles charged into the container to form a bed. Then made the bed vigorously fluidized for a few minutes to break down any particle interlocking. The pressure drop across the bed was measured as the fluidizing gas velocity reduced in stages. At higher gas flow rates, the pressure drop is less than the weight of the bed per unit area, because the column wall through particle–wall interactions is supporting some of the weight of the bed. At low gas flow rates, the pressure drop across the bed increases from zero gas flow rate, linearly, by increasing superficial gas velocity, until the bed approaches the conditions of fluidization. All experiments and simulations have been repeated multiple times. Table 7 represents the experimental results and the numerical values of minimum fluidization velocities, calculated by DPM associated with these drag models. These numerical values compared with experimental results obtained from the fluidized bed unit H692. Deviations of numerical values from the experimental results are represented in Table 8. The numerical results are in a very good agreement with experimental data.

Table 9 represents that the numerical values of minimum fluidization velocities have been calculated by different drag models that are compared with experimental results of Gunn and Hilal [1]. They provided u_{mf} values of particles with different diameters (100, 325, 500, and 1000 μm) and different densities (1228 and 2950 kg/m^3) in a cylindrical bed with the diameter of 89 mm. Deviations of numerical values from the empirical data are represented in Table 10. These empirical data also confirm the accuracy of the simulations.

4.2 Effect of drag model

One of the predominant forces between the gas phase and the particulate phase is the drag force. The drag functions

Table 6 Properties of granular material

Properties	Pack 1	Pack 2	Pack 3	Pack 4	Pack 5	Pack 6	Pack 7	Pack 8	Pack 9
Average particle diameter (μm)	100	125	150	175	200	225	250	275	300
Minimum particle diameter (μm)	67	74	106	125	134	158	177	204	247
Maximum particle diameter (μm)	140	194	236	274	315	372	390	413	488
Density of granular material (kg/m^3)	3770	3770	3770	3770	3770	3770	3770	3770	3770

Table 7 Comparisons of different u_{mf} values calculated by different drag models with the experimental values

ρ_p (kg/m^3)	d_p (μm)	Cheremisinoff	Kelessidis	Morsi	Richardson	Schiller	Clift	Dallavale	Ihme	Experimental
3770	100	0.0245	0.0239	0.0241	0.023	0.0237	0.0226	0.0203	0.0205	0.027
3770	125	0.0372	0.0372	0.0369	0.0363	0.0349	0.0354	0.0339	0.0327	0.038
3770	150	0.0526	0.0481	0.0456	0.0452	0.0447	0.0449	0.0459	0.0477	0.053
3770	175	0.074	0.074	0.0692	0.0671	0.0662	0.0672	0.0626	0.0615	0.072
3770	200	0.0813	0.0792	0.0828	0.0791	0.0845	0.0801	0.0814	0.0828	0.091
3770	225	0.103	0.1006	0.1025	0.0935	0.1033	0.093	0.0706	0.0736	0.112
3770	250	0.1485	0.1232	0.1201	0.1198	0.1198	0.1201	0.111	0.112	0.140
3770	275	0.166	0.1486	0.1563	0.1643	0.159	0.1683	0.162	0.1647	0.179
3770	300	0.206	0.1935	0.1953	0.2111	0.2098	0.2139	0.2042	0.2060	0.232

Table 8 Deviations of different drag models from experimental values for prediction of u_{mf}

ρ_p (kg/m^3)	d_p (μm)	Errors (%)							
		Cheremisinoff	Kelessidis	Morsi	Richardson	Schiller	Clift	Dallavale	Ihme
3770	100	9.3	11.5	10.7	15	12	16.2	25	24.1
3770	125	2	2	2.9	4.5	8	6.8	10.8	13.9
3770	150	7	9.2	14	14.8	15.7	15.2	13.4	10
3770	175	2.78	2.8	3.8	6.8	8	6.7	13	14.5
3770	200	10.7	13	9	13.1	7.1	12	10.6	9
3770	225	8.4	10.2	8.5	16.5	7.8	17	37	34.3
3770	250	6	12	14.2	14.4	14.4	14.2	20.7	20
3770	275	9	17	12.7	8.2	11.2	6	9.5	8
3770	300	11.3	16.6	15.8	9	9.6	7.8	12	11.2

Table 9 Comparison of different u_{mf} values calculated by different drag models with the experimental values [1]

ρ_p (kg/m^3)	d_p (μm)	u_{mf} (m/s)								
		Cheremisinoff	Kelessidis	Morsi	Richardson	Schiller	Clift	Dallavale	Ihme	Experimental
1228	232	0.0417	0.0417	0.0398	0.0385	0.0384	0.0385	0.0359	0.0352	0.0462
2950	100	0.0186	0.0186	0.0186	0.0185	0.0180	0.0182	0.0177	0.0172	0.021
2950	325	0.1451	0.1569	0.1482	0.1467	0.1476	0.1478	0.1369	0.1396	0.1572
2950	500	0.2706	0.2565	0.2787	0.2746	0.2759	0.2711	0.2542	0.271	0.285
2950	1000	0.6227	0.5665	0.6394	0.6440	0.6312	0.6184	0.5865	0.6630	0.6373

Table 10 Deviations of different drag models from experimental values of Gunn and Hilal [1]

ρ_p (kg/m^3)	d_p (μm)	Errors (%)							
		Cheremisinoff	Kelessidis	Morsi	Richardson	Schiller	Clift	Dallavale	Ihme
1228	232	9.7	9.7	13.8	16.67	18	16.67	22	23.8
2950	100	11	11	11.4	11.9	14	13.3	15.7	18
2950	325	7.7	0.2	5.7	6.7	6.1	6	12.9	11.2
2950	500	5	10	2.2	3.6	3.2	4.9	10.8	4.9
2950	1000	2.3	11	0.3	1	1	3	8	4

for modeling the momentum exchange between the phases are mostly obtained experimentally. Therefore, their suitability to model a fluidized bed of specific flow regime needs to be evaluated.

The stationary drag correlation of Stokes [39] for submicron spherical particles is

$$C_{D_s} = \frac{24}{Re_s} Re_s \ll 1. \tag{19}$$

Oseen [39] extended Stokes equation to flow regimes with higher Reynolds numbers by considering inertia as

$$C_{D_s} = \frac{24}{Re_s}\left(1 + \frac{3}{16} Re_s\right) \quad Re_s < 3. \tag{20}$$

Kelessidis [26] provided an extra expression for currents occur within a broad range of Reynolds numbers ($1 < Re_s < 500$) and the drag coefficient remains almost constant for Reynolds numbers beyond that ($Re_s > 500$). This drag function underestimates the minimum fluidization velocities by an average factor of 0.93. Schiller and Naumann [27] provided an empirical correlation for $Re_s < 1000$. Values of the drag coefficients coincide with 0.44 for spherical particles with $Re_s > 1000$. This model has a good stability and convergence. However, it underpredicts the values of u_{mf} by an average factor of 0.91. The stationary drag correlation of Dallavale [28] is presented for the flow regimes with Reynolds numbers less than

2×10^5. Despite its good stability and convergence, the deviation of this model from experimental data is more than other models. Morsi and Alexander [29] model is the most complete, adjusting correlation that is defined over a large range of Reynolds numbers, but computations using this model may be less stable than the others. Clift et al. [30] suggested a model for a large range of Re_s that has been divided into ten subintervals, with a distinct correlation for each interval. Since particles Reynolds numbers in this work do not exceed from 50, only the first three of these intervals are represented in Table 2. It underpredicts the values of u_{mf} by an average factor of 0.91 as Schiller and Naumann [27] model. Ihme drag correlation [31] is only provided for the regimes with $Re_s < 10^4$. This model predicts lower drag coefficient than the others, especially in small Reynolds numbers. The values of drag coefficients calculated by Khan and Richardson [33] drag model are very close to the values of Clift et al. [30] model. Cheremisinoff and Gupta [32] drag model is the most stable, complete and adjusting model that is presented for a large range of Reynolds numbers. It has the least runtime and the values calculated by this model have the least deviation from experimental values. Holzer and Sommerfeld [20] drag model is one of the most popular drag models for non-spherical particles due to its simplicity and general applicability. By considering the comparisons between the numerical results and experimental data (Tables 7, 8, 9, 10, 15, 16) and due to the runtime of each drag model, the drag correlations of Cheremisinoff and Gupta [32] and Holzer and Sommerfeld [20] were selected to simulate the drag forces of spherical and non-spherical particles, respectively.

4.3 Effect of gas holdup

The gas holdup (void fraction) which is one of the most important hydrodynamic parameters in fluidization phenomenon, depends mainly on the velocity and physical properties of the particulate phase such as average size or the distribution of the particles. It also governs the gas velocity in the vessel, turbulence characteristics of each phase and the energy dissipation rates. Thus, determination of the initial gas holdup is important to perform a better simulation. The gas holdup or the gas volume fraction indicates the free spaces between particles that are occupied by the gas. The gas holdup increases as the superficial gas velocity increases. This is clear, as the volume of air increases, more space will be occupied by the gas. The distribution of solid particles is not always similar to that of gas–particle interaction force, because the value of gas–particle interaction force depends on the relative velocity between two phases in addition to the void fraction. When gas is distributed through the bed, particles near the wall often lift up with lower velocities than those in the center due to the fluid–wall friction (non-slip conditions). Thus, particles distribution would be denser near the wall and create a large resistance force to gas flow. As gas flows through the bed center, more particles accumulate near the wall. Therefore, the most particle–particle collisions occur in high solid concentration zones near the wall. Besides, when particles (especially those at the bottom and near the wall) get closer to each other, there would be less space occupied by the gas phase, so the gas holdup decreases. Consequently, the drag force between particulate phase and gas phase increases, which decreases the minimum fluidization velocity. Overall, void fraction, particle interactions, and drag force are three factors that highly affect each other and cannot be studied separately. If the particles are perfectly spherical and completely stick together, the amount of the gas holdup would be 0.4 [36]. The gas holdup required to obtain the minimum fluidization velocity of spherical particles is reported between 0.4 and 0.45 in most experiments [1–9]. Table 11 represented the values of the minimum fluidization velocities have been calculated by different gas holdups in this range. Minimum fluidization velocity increases by increasing the gas holdup. The effect of the gas holdup is more intense in small diameters; however, it does not depend on the density of the particles. The same study has been performed for non-spherical particles and the results are shown in Table 12. Comparisons between the numerical values and the experimental data (from both experimental cases) for spherical and non-spherical particles are represented in Tables 13 and 14, respectively. According to these deviations, the minimum gas holdup needed for occurring incipient fluidization is 0.44 and 0.54 for spherical and non-spherical particles, respectively.

4.4 Effects of particle diameter and density

According to numerous experimental studies have been carried out recently, minimum fluidization velocity depends on bed geometry and properties of particles. In this work, the effects of particle sphericity, diameter, and density on the minimum fluidization velocity have been investigated. Comparisons between the numerical values of the minimum fluidization velocities at different diameter ratios with different density ratios and the values obtained from both empirical cases are shown in Fig. 2. The values of the minimum fluidization velocities were determined from the model developed in this study represent a very good agreement with the experimental results. As it can be seen in Fig. 3, minimum fluidization velocity increases with increasing the diameter ratio. Due to the increasing incline of each graph (in a constant density ratio), the effect

Table 11 Values of minimum fluidization velocities calculated by different gas holdups for spherical particles

ρ_p (kg/m^3)	d_p (μm)	u_{mf} (m/s)						
		$\varepsilon = 0.4$	$\varepsilon = 0.41$	$\varepsilon = 0.42$	$\varepsilon = 0.43$	$\varepsilon = 0.44$	$\varepsilon = 0.45$	Experimental
1228	232	0.0267	0.03	0.0335	0.0374	0.0417	0.0463	0.0462
2950	100	0.0118	0.0133	0.015	0.0166	0.0186	0.0206	0.021
2950	325	0.0987	0.109	0.1202	0.1322	0.1451	0.1583	0.1572
2950	500	0.1897	0.2082	0.2278	0.2487	0.2706	0.2939	0.285
2950	1000	0.4550	0.494	0.5346	0.5777	0.6227	0.6694	0.6373
3770	100	0.0153	0.0186	0.0205	0.0245	0.0266	0.0291	0.027
3770	125	0.0236	0.0266	0.0299	0.0333	0.0372	0.0413	0.038
3770	150	0.0258	0.0293	0.0344	0.0421	0.0507	0.0586	0.053
3770	175	0.0476	0.0534	0.0598	0.0668	0.074	0.0829	0.072
3770	200	0.0612	0.0683	0.0774	0.0835	0.0881	0.0943	0.091
3770	225	0.0521	0.0767	0.0844	0.0912	0.107	0.1341	0.112
3770	250	0.0812	0.1066	0.1194	0.1334	0.1485	0.1652	0.140
3770	275	0.1210	0.1421	0.1576	0.1634	0.1722	0.1992	0.179
3770	300	0.1745	0.1872	0.1921	0.2066	0.2143	0.2763	0.232

Table 12 Values of minimum fluidization velocities calculated by different gas holdups for non-spherical particles

d_v (mm)	ρ_p (kg/m^3)	φ	$\varphi_\perp$	u_{mf} (m/s)					
				$\varepsilon = 0.51$	$\varepsilon = 0.52$	$\varepsilon = 0.53$	$\varepsilon = 0.54$	$\varepsilon = 0.55$	Experimental
7	708.5	0.87	1.32	11.23	10.96	10.60	9.56	10.52	9.8
5	719.3	0.87	1.563	11.77	11.41	11.07	8.78	11.15	9.8
7	746.9	0.80	1.175	11.38	11.03	10.69	9.11	10.50	9.7
5	760.4	0.78	2.78	12.90	12.58	11.38	11.20	11.51	10.3
7	739.7	0.73	2.18	12.61	12.39	11.78	11.50	11.71	10.3
5	745.6	0.75	2.18	13.64	13.49	13.29	9.95	13.41	11.5
7	672.8	0.63	1.94	11.29	11.16	10.79	10.45	11.33	10.2
5	754.1	0.71	2.00	12.99	12.82	12.48	9.23	12.59	10.8
7	721.7	0.58	3.21	13.63	13.54	13.33	13.15	13.37	11.7
5	756.6	0.69	2.45	14.55	14.34	14.07	10.38	14.19	12.1
5	728.1	0.64	3.27	14.59	15.28	13.78	11.56	13.61	12.4

Table 13 Deviations of u_{mf} values for spherical particles calculated by different gas holdups from experimental values

ρ_p (kg/m^3)	d_p (μm)	Errors (%)					
		$\varepsilon = 0.4$	$\varepsilon = 0.41$	$\varepsilon = 0.42$	$\varepsilon = 0.43$	$\varepsilon = 0.44$	$\varepsilon = 0.45$
1228	232	42	35	27	19	9.7	0.2
2950	100	44	37	28.5	21	11	1.9
2950	325	37	31	23.5	16	7.7	0.7
2950	500	33	27	20	13	5	3
2950	1000	28.6	22.5	16	9	2.3	5
3770	100	43.3	31.1	24	9.3	1.5	7.77
3770	125	38	30	21.3	12	2	8.7
3770	150	51.3	44.7	35.1	20.6	4.3	10.6
3770	175	33.9	25.8	16.9	7	2.8	15
3770	200	32.7	24.9	14.9	8.2	3.2	3.6
3770	225	53.4	31.5	24.6	18.6	4.5	17.3
3770	250	42	23.8	14.7	4.7	6	18
3770	275	32.4	20.6	12	8.7	3.8	11.3
3770	300	24.8	19.3	17.2	11	7.6	19

Table 14 Deviations of u_{mf} values for non-spherical particles calculated by different gas holdups from experimental values

d_v (mm)	ρ_p (kg/m^3)	φ	$\varphi_\perp$	Error (%)					
				$\varepsilon = 0.51$	$\varepsilon = 0.52$	$\varepsilon = 0.53$	$\varepsilon = 0.54$	$\varepsilon = 0.55$	Experimental
7	708.5	0.87	1.32	14.61	11.85	8.19	2.4	7.31	9.8
5	719.3	0.87	1.563	20.12	16.45	12.94	10.4	13.83	9.8
7	746.9	0.80	1.175	17.32	13.67	10.16	6	8.23	9.7
5	760.4	0.78	2.78	25.27	22.14	10.55	8.7	11.78	10.3
7	739.7	0.73	2.18	22.46	20.29	14.36	11.6	13.73	10.3
5	745.6	0.75	2.18	18.62	17.33	15.58	13.5	16.64	11.5
7	672.8	0.63	1.94	10.73	9.42	5.76	2.4	4.88	10.2
5	754.1	0.71	2.00	20.32	18.66	15.54	14.5	16.53	10.8
7	721.7	0.58	3.21	16.47	15.72	13.91	12.4	14.31	11.7
5	756.6	0.69	2.45	20.22	18.53	16.32	14.2	17.25	12.1
5	728.1	0.64	3.27	17.68	23.22	11.17	6.8	9.78	12.4

of particle diameter on the minimum fluidization velocity is more intense in larger diameter ratios and this effect will be attenuated by increasing the density ratio. The graph of the largest density ratio is a straight line then it turns to a curve that its incline decreases by decreasing the density ratio. If the density ratio becomes n times larger, the incline of the graph would increase $c \times n$ times. The coefficient of c can be between 0.75 and 0.9. As the density ratio increases, the coefficient of c decreases. Increasing the diameter of the particle causes the relative Reynolds number to increase. The distribution of the solid particles so as the void fraction also increases by increasing the diameter of particles. Since the drag force between the gas phase and the particulate phase depends on the relative Reynolds number and void fraction, it decreases by increasing these two factors. By decreasing the gas–particle interaction force, the minimum fluidization velocity increases. Figure 3 shows the effect of density ratio on the minimum fluidization velocity under different diameter ratios. It represents that minimum fluidization velocity increases with increasing the density ratio. Due to the decreasing incline of each diagram (in a constant diameter ratio), the effect of particle density on the minimum fluidization velocity is more sensitive to smaller density ratios and this effect will be intensified by increasing the diameter ratio. The graph of the smallest diameter ratio is a straight line, and then, it turns to a curve that its incline increases by increasing the diameter ratio. Increasing the density of the particles causes the relative Reynolds number to increase. However, the void fraction stays almost constant (before the incipient fluidization, when all the particles rest on one another), since the space occupied by the gas phase would not change by increasing the density of the particles. As the relative Reynolds number increases, the drag force between the gas phase and the particulate phase decreases. By decreasing the gas–particle interaction force, the minimum fluidization velocity increases.

Results show that by 25% enhancement in diameter and density of particles, the minimum fluidization velocity increases 94 and 27%, respectively. The effect of particle diameter is almost three times larger than density impact, which was predictable. Besides, the diameter of particles affects both the gas holdup and the relative Reynolds number, so the variation of particle diameter has a stronger impact on the minimum fluidization velocity than particle density. Comparing the numerical results with the experimental values of minimum fluidization velocity represented that the average deviation is about 6%, which proves that this is an applicable model to simulate the gas–solid fluidized bed.

4.5 Effect of particle sphericity

Another important parameter that has a considerable influence on the minimum fluidization velocity is the shape of particles. In this paper, the effect of the sphericity is considered in the expression of the drag equation for a better predication in practical application. Fluidization of non-spherical particles has been investigated using the model developed in this work. The drag correlation of Holzer and Sommerfeld [20] has been implemented to simulate the drag forces of non-spherical particles. Figure 4 represents the minimum fluidization velocity of non-spherical particles with the crosswise sphericity of 1.32, the density of 708.5 kg/m^{3,} and the diameters of 7 and 5 mm as a function of sphericity (φ). Figure 5 shows the minimum fluidization velocity of non-spherical particles with the sphericity of 0.87, the density of 708.5 kg/m^{3,} and the diameters of 7 and 5 mm as a function of crosswise sphericity ($\varphi_\perp$). Non-spherical particles reach the minimum fluidization velocity at lower gas velocities in

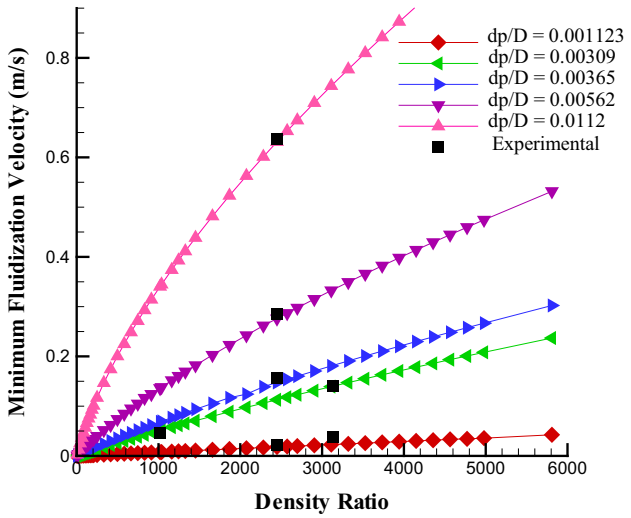

Fig. 3 Effect of density ratio on the minimum fluidization velocity under different diameter ratios

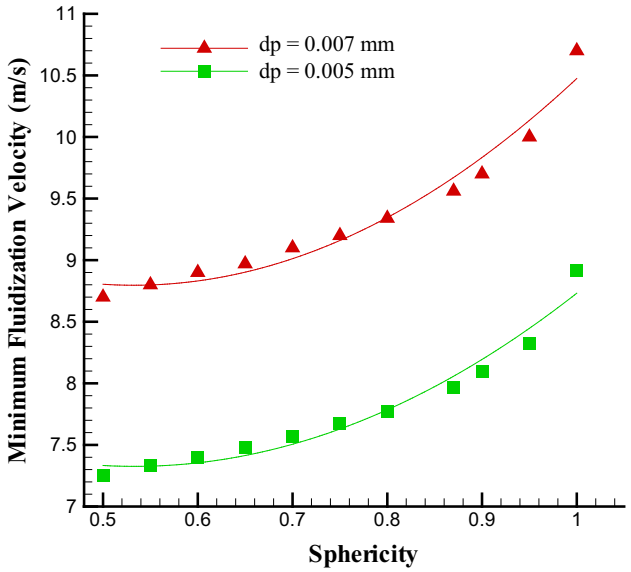

Fig. 4 Minimum fluidization velocity as a function of sphericity

comparison with spherical particles. As the shape of the particles approaches to sphere and the coefficients of sphericity and crosswise sphericity increase, the minimum fluidization velocity increases. The minimum fluidization velocity would increase 12.5% with 25% increase of the crosswise sphericity. This enhancement in lower values of sphericity is about 3.5% per 25% increase of sphericity but it becomes more intense (7% increase) from the sphericity of 0.95–1.00, where the particle shape completely changes to sphere. On the other hand, for particles with shapes that are so much different from that of a sphere, complete fluidization occurs at higher velocities with decreasing sphericity. At low gas velocities, particles with lower

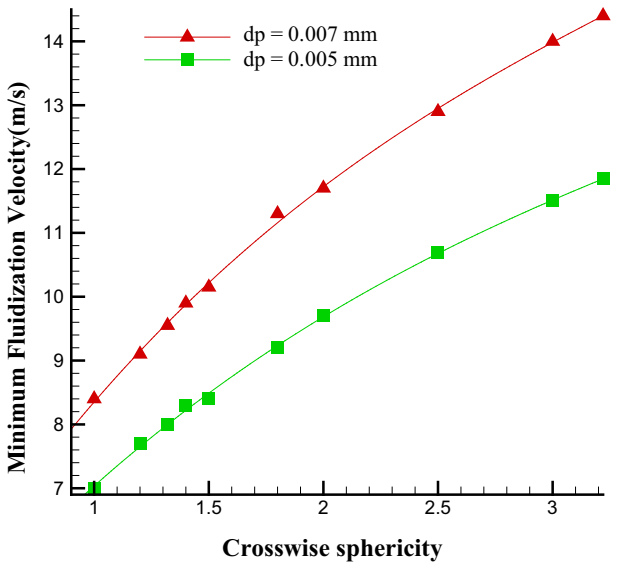

Fig. 5 Minimum fluidization velocity as a function of crosswise sphericity

sphericity have tendency to form channels which cause a lower pressure drop, because not all particles are completely suspended. Besides, non-spherical particles move faster through the fluid flow than the spherical particles, since they tend to increase the drag force, by aligning their longest axis perpendicular to the fluid flow direction. Table 15 represents the comparisons between the numerical values of the minimum fluidization velocity calculated by different drag models and the experimental values of Kruggel-Emden and Vollmari [10]. The numerical results of non-spherical particles with the drag model of Holzer and Sommerfeld [20] and the gas holdup of 54% are in good agreement with experimental data of Kruggel-Emden and Vollmari [10] within an average error of 9%, as it is shown in Table 16. The experimental results of Anantharaman et al. [8] also confirm the numerical investigation of particle diameter, density, and sphericity in the present study.

5 Conclusion

In this work, a new numerical model is proposed to investigate the minimum fluidization velocity of a cylindrical gas–solid fluidized bed in a broad range of particle diameter and particle density. This model predicts the values of the minimum fluidization velocity of both spherical and non-spherical particles very well within an average error of 6 and 9%, respectively. Different drag models have been examined and based on comparisons with experimental data the drag correlations of Cheremisinoff and Gupta [32] and Holzer and Sommerfeld

Table 15 Comparisons between the numerical values of u_{mf} and the experimental values of Kruggel-Emden and Vollmari [10]

d_v (mm)	ρ_p (kg/m^3)	φ	$\varphi_\perp$	u_{mf} (m/s)					
				Holzer	Swamee	Ganser	Haider	Chien	Experimental
7	708.5	0.87	1.32	9.56	10.91	13.19	11.15	13.65	9.8
5	719.3	0.87	1.563	8.78	11.9	16.08	12.21	14.38	9.8
7	746.9	0.80	1.175	9.11	11.81	12.93	15.1	12.49	9.7
5	760.4	0.78	2.78	11.20	12.49	16.01	14.76	15.87	10.3
7	739.7	0.73	2.18	11.50	15.22	11.66	15.21	14.64	10.3
5	745.6	0.75	2.18	9.95	14.04	13.08	12.92	15.58	11.5
7	672.8	0.63	1.94	10.45	11.39	11.27	11.80	15.53	10.2
5	754.1	0.71	2.00	9.23	13.80	13.45	11.93	12.78	10.8
7	721.7	0.58	3.21	13.15	15.76	16.10	18.42	15.49	11.7
5	756.6	0.69	2.45	10.38	16.64	16.75	17.63	17.85	12.1
5	728.1	0.64	3.27	11.56	14.06	18.02	16.31	13.69	12.4

Table 16 Deviation of different drag models from experimental values

d_v (mm)	ρ_p (kg/m^3)	φ	$\varphi_\perp$	Error (%)				
				Holzer	Swamee	Ganser	Haider	Chien
7	708.5	0.87	1.32	2.4	11.3	34.66	13.78	39.32
5	719.3	0.87	1.563	10.4	22.65	64.12	24.56	46.73
7	746.9	0.80	1.175	6	14.66	33.27	55.67	28.72
5	760.4	0.78	2.78	8.7	21.26	55.43	43.32	54.11
7	739.7	0.73	2.18	11.6	32.39	13.23	47.68	42.17
5	745.6	0.75	2.18	13.5	37.64	13.78	12.33	35.46
7	672.8	0.63	1.94	2.4	11.7	10.48	15.72	52.26
5	754.1	0.71	2.00	14.5	27.81	24.55	10.47	18.32
7	721.7	0.58	3.21	12.4	34.67	37.64	57.41	32.43
5	756.6	0.69	2.45	14.2	37.53	38.45	45.68	47.56
5	728.1	0.64	3.27	6.8	13.41	45.33	31.56	10.39

[20] were selected to simulate the drag forces of spherical and non-spherical particles, respectively. The minimum gas holdup needed for occurring incipient fluidization is determined 0.44 for spherical particles and 0.54 for non-spherical particles due to the comparisons between the empirical values and the numerical values have been calculated by different gas holdups. The effects of particle density and particle diameter on the minimum fluidization velocity are more intense in small density ratio and large diameter ratio, respectively. Results showed that by 25% enhancement in diameter, density and crosswise sphericity and sphericity of particles, the minimum fluidization velocity increases 94, 27, 12.5, and 3.5%, respectively. Besides, the diameter of particles affects both the gas holdup and the relative Reynolds number, so the variation of particle diameter has a stronger impact on the minimum fluidization velocity than particle density. Non-spherical particles reach the minimum fluidization velocity at lower gas velocity. The minimum fluidization velocity increases by increasing the coefficients of sphericity and crosswise sphericity, but complete fluidization occurs at higher velocities with decreasing sphericity for particles with shapes that are so much different from that of a sphere.

References

1. Gunn DJ, Hilal N (1997) The expansion of gas-fluidised beds in bubbling fluidisation. Chem Eng Sci 52:11–22
2. Escudero D, Heindel TJ (2011) Bed height and material density effects on fluidized bed hydrodynamics. Chem Eng Sci 66:3648–3655
3. Caicedo GR, Ruiz MG, Marques JJP (2002) Minimum fluidization velocities for gas–solid 2D beds. Chem Eng Process 41:761–764
4. Sau DC, Mohanty S, Biswal KC (2007) Minimum fluidizations velocities and maximum bed pressure drops for gas–solid tapered fluidized beds. Chem Eng J 132:151–157
5. Gupta SK, Agarwal VK, Singh SN, Seshadri V, Mills D, Singh J, Prakash Ch (2009) Prediction of minimum fluidization velocity for fine tailings materials. Powder Technol 196:263–271

6. Delgado S, Almendros JA, Hernando N, Santana D (2011) On the minimum fluidization velocity in 2D fluidized bed. Powder Technol 207:145–153
7. Farhadi F, Rasteh M, Bahramian A (2015) Hydrodynamic characteristics of gas–solid tapered fluidized beds: experimental studies and empirical models. Powder Technol 283:355–367
8. Anantharaman A, Cahyadi A, Hadinoto K, Chew JW (2016) Impact of particle diameter, density and sphericity on minimum pick up velocity of binary mixtures in gas–solid pneumatic conveying. Powder Technol 297:311–319
9. Asif M (2013) Predicting minimum fluidization velocities of multi-component solid mixtures. Particuology 11:309–316
10. Kruggel-Emden H, Vollmari K (2016) K flow-regime transitions in fluidized beds of non-spherical particles. Particuology 29:1–15
11. Pain CC, Mansoorzadeh S, de Oliveira CRE (2001) A study of bubbling and slugging fluidised beds using the two-fluid granular temperature model. Int J Multiph Flow 27:527–551
12. Zhao Y, Tang L, Luo Z, Liang C (2010) Experimental and numerical simulation of the fluidization characteristics of a separating gas–solid fluidized bed. Fuel Process Technol 91:1819–1825
13. Mostafazadeh M, Rahimzadeh H, Hamzei M (2013) Numerical analysis of the mixing process in a gas–solid fluidized bed reactor. Powder Technol 239:422–433
14. Sau DC, Biswal KC (2011) Computational fluid dynamics and experimental study of the hydrodynamics of a gas–solid tapered fluidized bed. Appl Math Model 35:2265–2278
15. Pedroso FA, Zinani F, Indrusiak MLS (2016) Numerical study of circulating fluidized beds built using Glicksman's simplified and full sets of scaling parameters. J Braz Soc Mech Sci Eng 38:2085
16. Liu X, Zhu C, Geng S (2015) Two-fluid modeling of Geldart A particles in gas–solid micro-fluidized beds. Particuology 21:118–127
17. Gera D, Gautam M, Tsuji Y, Kawaguchi T, Tanaka T (1998) Computer simulation of bubbles in large-particle fluidized beds. Powder Technol 98:38–47
18. Kobayashi N, Yamazaki R, Mori S (2000) A study on the behavior of bubbles and solids in bubbling fluidized beds. Powder Technol 113:327–344
19. Deen NG, Van Sint Annaland M, Van der Hoef MA, Kuipers JAM (2007) Review of discrete particle modeling of fluidized beds. Chem Eng Sci 62:28–44
20. Holzer A, Sommerfeld M (2008) New simple correlation formula for the drag coefficient of non-spherical particles. Powder Technol 184:361–365
21. Di Felice R (1994) The voidage function for fluid–particle interaction systems. Int J Multiph Flow 20:153–159
22. Hilton JE, Mason LR, Cleary PW (2010) Dynamics of gas–solid fluidised beds with non-spherical particle geometry. Chem Eng Sci 65:1584–1596
23. Zhou ZY, Pinson D, Zou RP, Yu AB (2011) Discrete particle simulation of gas fluidization of ellipsoidal particles. Chem Eng Sci 66:6128–6145
24. Ganser GH (1993) A rational approach to drag prediction of spherical and non-spherical particles. Powder Technol 77:143–152
25. Moffat RJ (1988) Describing the uncertainties in experimental results. Exp Therm Fluid Sci 1:3–17
26. Kelessidis VC (2003) Terminal velocity of solid spheres falling in Newtonian and non Newtonian liquids. Sci J Tech Chamb Greece 23:43–54
27. Shiller L, Naumann A (1935) A drag coefficient correlation. Zeitschrift des Vereins Deutscher Ingenieure 77:318–320
28. Dallavalle JM (1948) Micromeritics: the technology of fine particles, 2nd edn. Pitman, London
29. Morsi SA, Alexander AJ (1972) An investigation of particle trajectories in two-phase flow systems. J Fluid Mech 55:193–208
30. Clift R, Grace JR, Weber ME (1978) Bubbles, drops, and particles. Academic Press, New York
31. Ihme F, Schmidt-Traub H, Brauer H (1972) Theoretical study of the flow around and the mass transfer at balls. Chem Eng Tecnol 44:306–313
32. Cheremisinoff N, Gupta R (1983) Handbook of fluids in motion. Ann Arbor Science, Michigan
33. Khan AR, Richardson JF (1987) The resistance to motion of a solid sphere in a fluid. Chem Eng Commun 62:135–150
34. Swamee PK, Ojha CSP (1991) Drag coefficient and fall velocity of nonspherical particles. J Hydraul Eng 117:660–667
35. Chien SF (1994) Settling velocity of irregularly shaped particles. SPE Drill Complet 9:281–289
36. Haider AM, Levenspiel O (1989) Drag coefficient and terminal velocity of spherical and nonspherical particles. Powder Technol 58:63–70
37. Torfeh S, Kouhikamali R (2015) Numerical investigation of mist flow regime in a vertical tube. Int J Therm Sci 95:1–8
38. Isbin HS (1970) One dimensional two phase flow, Graham B. Wallis, vol 16. McGraw-Huill, New York, pp 896–1105. https://doi.org/10.1002/aic.690160603
39. Ounis H, Ahmadi G, McLaughlin JB (1991) Brownian diffusion of submicrometer particles in the viscous sublayer. J Colloid Interface Sci 143:266–277